Piezospectroscopy of the $p_{3/2}$ and Fano series of singly ionized zinc in germanium

G. Piao, P. Fisher, and R. A. Lewis
Department of Physics, University of Wollongong, Wollongong, New South Wales 2522, Australia
(Received 15 October 1999)

The absorption spectrum of singly ionized zinc in Ge has been studied using Fourier spectroscopy. Improved experimental conditions give more details for the $p_{3/2}$ series than previously. Quantitative piezospectroscopy has been performed with compression along $\langle 111\rangle$ and $\langle 100\rangle$. It is deduced that the final states of the compound C line include $1\Gamma_7^-$, $3\Gamma_8^-$, $3\Gamma_8^+$, and $4\Gamma_8^+$. More reliable deformation potential constants of some energy states have been obtained. Fano resonances associated with bound-hole states have been studied with and without applied uniaxial compression. The piezospectroscopic behavior of these is compared with that of the parent $p_{3/2}$ series.

I. INTRODUCTION

Since the first observation of their Lyman series,[1] the bound energy states of neutral acceptors in Ge have been investigated extensively both experimentally and theoretically, with and without external perturbations.[2–4] Acceptors studied include the group I element Cu; the group II elements Be, Mg, Zn, and Hg; and all the group III elements.[4] The hole bound to a shallow acceptor ion in Ge produces discrete states near the top of either the $j=3/2$ or the $j=1/2$ valence band. Unlike acceptors in Si, only one series of acceptor absorption lines, the $p_{3/2}$ series, has been observed for Ge, although the $p_{1/2}$ series is predicted.[5,6]

The $p_{3/2}$ series of singly ionized zinc, Zn^-, in Ge,[7–12] which will be denoted by Ge(Zn^-), exhibits the characteristics of the neutral acceptors, except that the binding energies of the excited states are ~4 times larger.[7,9,10] The $p_{3/2}$ series occurs in the spectral range 65–85 meV. Ge(Zn^-) also shows several asymmetric, broad features in the range 100–120 meV. These are Fano[13] resonances arising from interference between the $p_{3/2}$ band continuum and states compounded from bound-hole and localized zone-center optical phonon states.[12,14] The Fano features are represented by $(q+\varepsilon)^2/(1+\varepsilon^2)$, where ε, the reduced energy variable,[13,14] when zero, determines the energy of the resonance. The parameter q depends on the states involved in the transition. The larger its magnitude, the more asymmetric the resonance; $q=0$ is a pure antiresonance. Fano resonances have been observed for various dopants in Si and Ge;[15] however, Zn^- is the only known acceptor in Ge, involving bound holes, exhibiting these.[12,14] In this investigation, a systematic piezospectroscopic study of phonon-assisted Fano resonances of Ge(Zn^-) has been made. Results for a compressive force **F** along either $\langle 111\rangle$ or $\langle 100\rangle$ are presented. During the investigation of the stress-induced behavior of the Fano resonances, significant new and more precise data were obtained for the $p_{3/2}$ states, permitting a detailed description of the complex comprising the C line. These results will also be presented.

The symmetries of the states involved in the $p_{3/2}$ series are Γ_6, Γ_7, and Γ_8 of $\overline{T}_d$.[4,16] Under $\mathbf{F}\|\langle 111\rangle$, the two Kramers doublets represented by Γ_6 and Γ_7 each become Γ_4 of C_{3v}, the new impurity site symmetry, while Γ_8 states decompose into two doublets, Γ_4 and $\Gamma_5+\Gamma_6(\equiv\Gamma_{5+6})$ separated in energy by $\Delta'_{111}=(d'/\sqrt{3})s_{44}S$. Here d' is a deformation constant,[8] s_{44} is an elastic compliance coefficient, and S is the stress, which is positive for tension and negative for compression. With $\mathbf{F}\|\langle 100\rangle$, Γ_6 and Γ_7 of $\overline{T}_d$ become Γ_6 and Γ_7 of $\overline{D}_{2d}$, respectively, while Γ_8 reduces to Γ_6 and Γ_7 with an energy separation $\Delta'_{100}=2b'(s_{11}-s_{12})S$, where b' is another deformation constant[8] and s_{11} and s_{12} are elastic constants. Since the initial developments[17–20] of the theory of shallow acceptors in semiconductors, the treatment was significantly simplified by Baldereschi and Lipari,[21] who introduced a formalism by which the acceptor Hamiltonian could be separated into two parts, one with full spherical symmetry and the other with cubic symmetry. For almost all semiconductors, including Ge, the valence band parameters are such that the latter part is very much smaller than the former, permitting the cubic part to be treated as a perturbation. The cubic term reduces the symmetry from that of the full rotation group to $\overline{O}_h$,[16] the symmetry of the intrinsic material. Where convenient below, the notation based on $\overline{O}_h$ will be used for the unperturbed states since the retention of the parity labels makes it less cumbersome to be explicit. For example, the ground state of Zn^- is of Γ_8 symmetry under $\overline{T}_d$, the true site symmetry, while it is designated as Γ_8^+ under $\overline{O}_h$; the excited states of the G and D lines are also of Γ_8 symmetry under $\overline{T}_d$ but designated as Γ_8^- under $\overline{O}_h$. An integer is prefixed to the labels starting with 1 for the lowest energy state of a given symmetry. Thus, the unperturbed s-like ground state has the label $1\Gamma_8^+$ and higher-lying s-like states bear the labels $2\Gamma_8^+$, $3\Gamma_8^+$, etc., whereas the odd-parity Γ_8 excited states are $1\Gamma_8^-$, $2\Gamma_8^-$, etc., and so on. This labeling unambiguously distinguishes the unperturbed state from which a stress-induced state has emerged, while retaining the notation used in the group-theoretical treatment.[8]

II. EXPERIMENTAL PROCEDURES

The Ge samples were cut from single-crystal ingots deliberately double-doped with Sb and Zn to produce various con-

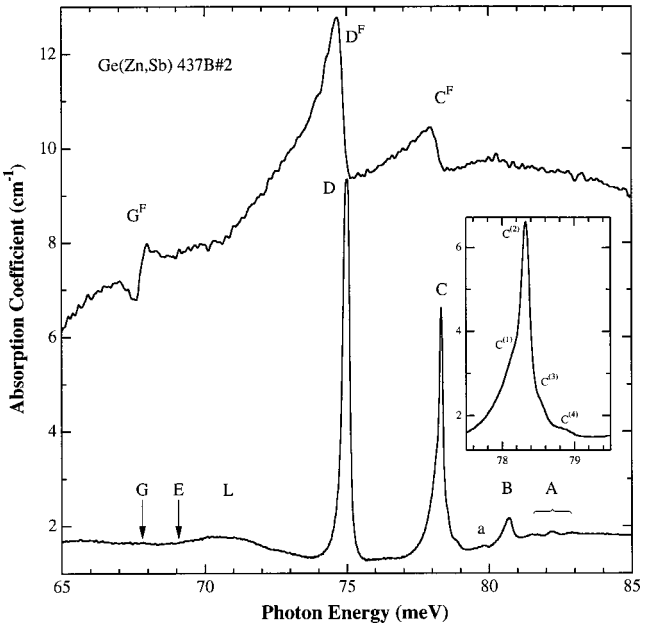

FIG. 1. Lower curve: The $p_{3/2}$ spectrum of Ge(Zn$^-$); L is a lattice band. Upper curve: The Fano spectrum of Ge(Zn$^-$) shifted down in energy by 37.83 meV, the energy of the zone-center optical phonon of Ge (Ref. 32) and expanded in the ordinate by 20 times, relative to the $p_{3/2}$ spectrum. Inset: Detail of the C line. Liquid helium was the coolant.

centrations of Zn$^-$ acceptors.[9,10] Uniaxial compressive forces were applied using either lead weights or a calibrated pressure head; the lower stresses were obtained with lead masses $\leqslant$60 kg. The low-temperature quantitative stress cryostat and sample-mounting procedure have been described elsewhere.[10,22] Absorption spectra were obtained using a BOMEM DA 3.26 Fourier transform infrared spectrometer. Liquid helium was used as coolant. All spectra shown were observed with a mirror travel of 2.5 cm, i.e., an unapodized resolution of $\sim$0.15 cm^{-1}. Where the spectral features were broader than this, smoothing was sometimes carried out to improve the signal-noise-ratio of the data. Cooled mercury cadmium telluride detectors were used. The radiation was linearly polarized with a gold-wire grid evaporated onto either a ZnSe or a polyethylene substrate.

III. EXPERIMENTAL RESULTS AND DISCUSSION

A. Unperturbed spectra

1. $p_{3/2}$ series

The unperturbed $p_{3/2}$ absorption spectrum of Ge(Zn$^-$) is shown in Fig. 1. The broad feature labeled L is a Ge lattice absorption band. The inset to Fig. 1 shows enlarged the features of the line conventionally labeled C for acceptors in Ge.[1,4] In addition to a strong central line there are three weak but identifiable shoulders evident, similar to those of Fig. 1 of BF76 (where convenient, Ref. 10 will be referred to as BF76). The four closely spaced transitions are labeled $C^{(1)}$, $C^{(2)}$, $C^{(3)}$, and $C^{(4)}$, in order of increasing energy. A similar set of C lines was observed for a sample with slightly higher Zn$^-$ concentration cut from a different ingot.[12] The transition energies of the four C lines have been obtained from a least-squares curve-fitting algorithm using Lorentzian line shapes[23] and are given in Table I. The energies of $C^{(1)}$, $C^{(2)}$, and $C^{(4)}$ agree with those reported in BF76 for C', C, and C'', respectively. The transition labeled $C^{(3)}$ has not been observed before. Theoretical calculations predict that for group III (Refs. 24, 25) and Zn$^-$ impurities,[26] the three states $1\Gamma_7^-$, $3\Gamma_8^-$, and $3\Gamma_8^+$, are very close in energy. The scaling factor between energy states of Zn$^-$ and group III impurities in Ge is $\sim$4.2,[10,12] so it might be expected that these states are sufficiently separated for Zn$^-$ that transitions to them can be resolved. The features $C^{(1)}$ and $C^{(2)}$ have been identified previously as having $3\Gamma_8^-$ and $1\Gamma_7^-$, respectively, as their final states.[12] The piezospectroscopic data given below indicate that $C^{(1)}$ has $3\Gamma_8^+$ as its excited state while the final state of $C^{(2)}$ is the combination $1\Gamma_7^- + 3\Gamma_8^-$. Calculations[26] suggest that $4\Gamma_8^+$ is the excited state of $C^{(3)}$.

TABLE I. Energies of some of the unperturbed transitions of Ge(Zn$^-$).

Line	Energy (meV)	Final state
G	67.80$\pm$0.01[a]	$1\Gamma_8^-$
	67.75$\pm$0.02[b]	
D	75.016$\pm$0.003	$2\Gamma_8^-$
$C^{(1)}$	78.107$\pm$0.007	$3\Gamma_8^+$
$C^{(2)}$	78.327$\pm$0.002	$1\Gamma_7^- + 3\Gamma_8^-$
$C^{(3)}$	78.57$\pm$0.02	$4\Gamma_8^+$
$C^{(4)}$	78.85$\pm$0.02	

[a]From piezospectroscopic measurements of the G_3 component (see text). The value obtained in this same manner by BF76 was 67.80$\pm$0.07 meV.

[b]From a sample with $\sim$4 times the concentration of the sample of Fig. 1.

The sample that yielded the spectrum of Fig. 1 was used to obtain Fig. 3 of BF76. This latter spectrum displays a very weak G line obtained by averaging a number of scans of the grating spectrometer used. In the present instance this very weak feature was not observed. All acceptors in Ge exhibit similar spectra.[4] The dominant lines are C and D with the G line being more than an order of magnitude weaker. For singly ionized acceptors Stark broadening is unavoidable and is known to become larger as the orbital of the excited state involved becomes larger.[4] The G line, a transition to the first excited state, should be the least affected and thus its absence is not attributed to this. A sample with $\sim$4 times the Zn$^-$ concentration of that of Fig. 1 exhibited a G line and also an E line. The energy of the former is given in Table I. The energies of the G and E lines are indicated in Fig. 1.

2. Fano series

The Fano series associated with the bound-hole transitions is also shown in Fig. 1; this series has been shifted down in energy by the energy of the zone-center optical phonon to illustrate its correlation with the $p_{3/2}$ spectrum. Figure 2 shows the Fano resonances of three other samples. The Zn$^-$ spectrum was used to gauge the relative concentrations of Zn$^-$ in these three samples. The values obtained for the parameters characteristic of each of the resonances G^F, D^F,

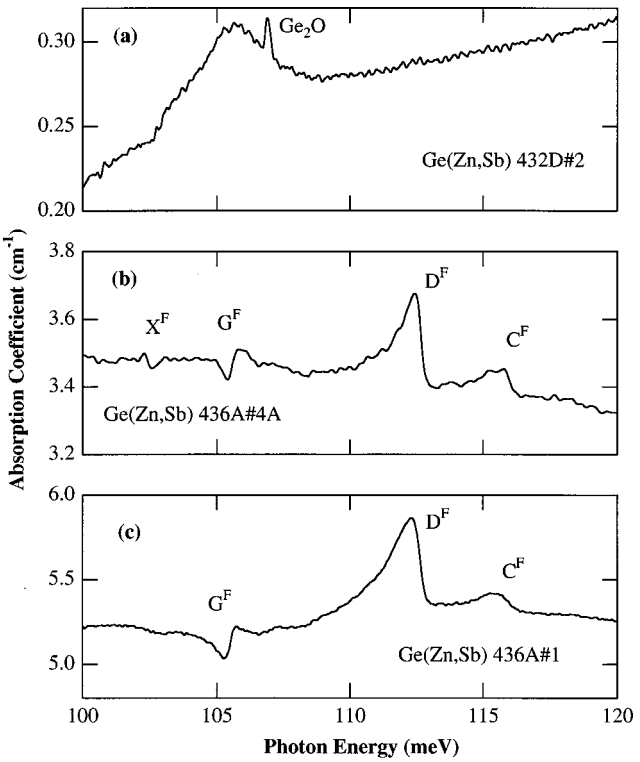

FIG. 2. Fano spectra of Ge(Zn$^-$) for concentrations in the ratios (a):(b):(c) of 1:55:155.

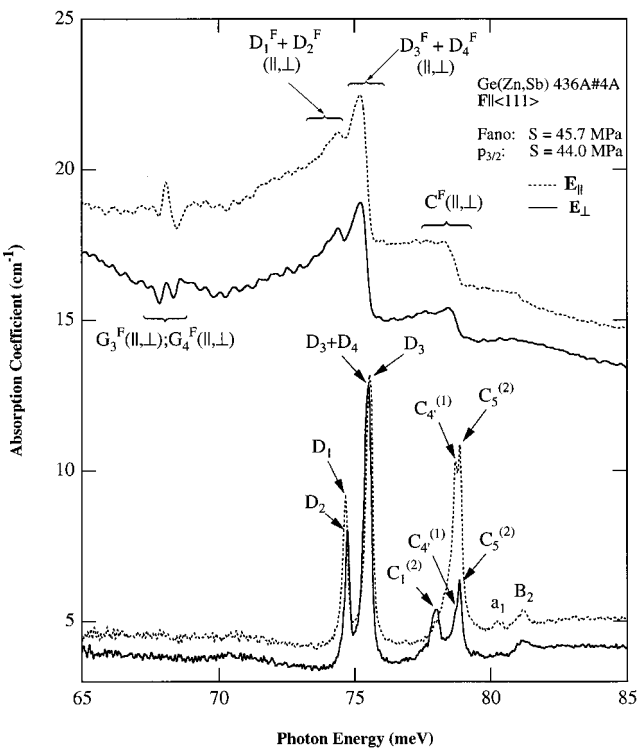

FIG. 3. Fano and $p_{3/2}$ spectra of Ge(Zn$^-$) for $\mathbf{F}\|\langle 111\rangle$. The Fano spectra (upper two curves) were measured at a stress of 45.7 MPa while the $p_{3/2}$ spectra (lower two curves) were measured at a stress of 44.0 MPa. The Fano spectra have been shifted down in energy by 37.83 meV. The axis at the left applies to the $p_{3/2}$ spectra; the Fano spectra have been scaled up in the ordinate by a factor of 20.

and C^F are given in Table II for three of the samples. More details are given elsewhere.[12,14]

B. Effects of uniaxial compression

Quantitative piezospectroscopic observations have been made with $\mathbf{F}\|\langle 111\rangle$ and $\langle 100\rangle$ and the electric vector $\mathbf{E}$ of the radiation polarized either parallel ($\mathbf{E}_\|$) or perpendicular ($\mathbf{E}_\perp$) to $\mathbf{F}$. Such studies have been reported previously[9,10] for the $p_{3/2}$ spectrum; only where either new features are observed or new labels are required will the present data be given. For the Fano resonances, preliminary results have been reported elsewhere.[12,27]

1. Applied force along a ⟨111⟩ axis

a. $p_{3/2}$ spectrum. Figure 3 shows the behavior of some of the lines of the $p_{3/2}$ series for $\mathbf{F}\|\langle 111\rangle$. Data for $\mathbf{E}_\|$ are shown as the dashed curve; data for $\mathbf{E}_\perp$ are the full curve. This figure may be compared with Fig. 5 of BF76. The component $C_{4'}^{(1)}$ was not reported in the previous work although examination of unpublished data reveals a hump and a shoulder on the low-energy side of C_5 (here relabeled $C_5^{(2)}$) for $\mathbf{E}_\|$ and $\mathbf{E}_\perp$, respectively. It is conjectured that in the previous work, even though the resolution was sufficient to separate $C_{4'}^{(1)}$ and $C_5^{(2)}$ for $\mathbf{E}_\|$, small fluctuations in the gas pressure providing the stress may have broadened the lines. Spectra obtained at other stresses are also very similar to those observed previously.

Figure 4 shows the stress dependence of the energies of components of lines *G*, *D*, and *C*. The subscripts given on the labels are those of BF76 except for $C_{4'}^{(1)}$. Results for lines *a* and *B* are not shown as they are identical to those reported earlier. For the *C* lines, the superscript identifies the parent *C* line; the assignments will be discussed later. In Fig. 4, the full curves are the results of least-squares fits and the data of BF76 have been included for the *G* line. The least-squares fits to all the data have been used to determine the zero-stress values. Because of the linear nature of the dependence of G_3 on stress, its intercept (see Table I) has been taken as the unperturbed energy of the *G* line. If the zero-stress value of the *D* line (see Table I) is omitted from the

TABLE II. Comparison of Fano parameters for Zn$^-$ in different Ge samples.

	G^F		D^F		C^F	
Sample	$h\upsilon_0$ (meV)	q	$h\upsilon_0$ (meV)	q	$h\upsilon_0$ (meV)	q
437B#2	105.53±0.02	0.80±0.10	112.65±0.01	−1.46±0.07	115.97±0.02	−1.36±0.07
436A#4A	105.51±0.01	0.75±0.04	112.63±0.02	−1.58±0.15	115.95±0.03	−1.5±0.2
436A#1	105.53±0.01	1.10±0.08	112.56±0.01	−1.56±0.20	115.85±0.02	−1.5±0.2

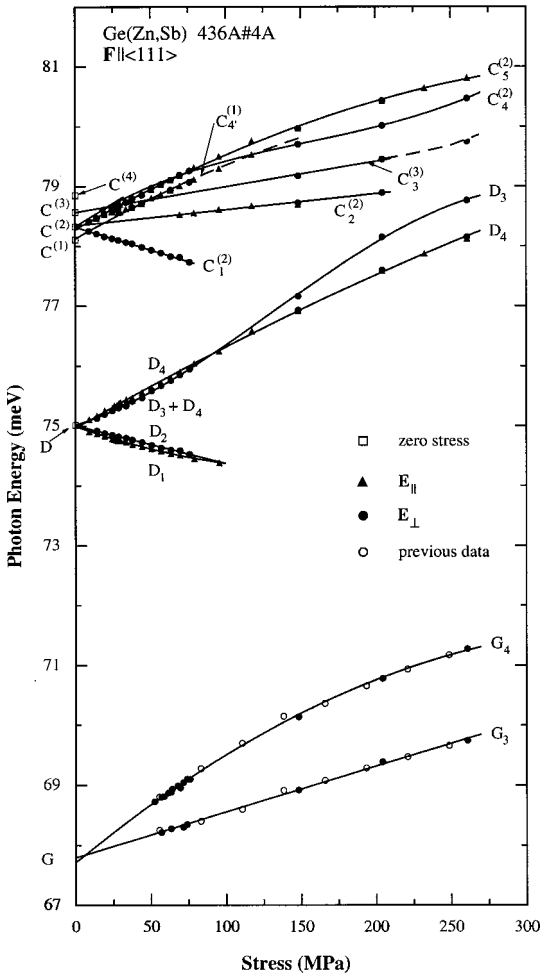

FIG. 4. Stress dependence of the *G*, *D*, and *C* components of Ge(Zn^-) for $\mathbf{F}\|\langle 111\rangle$. Data for the *G* line from Ref. 10 are included.

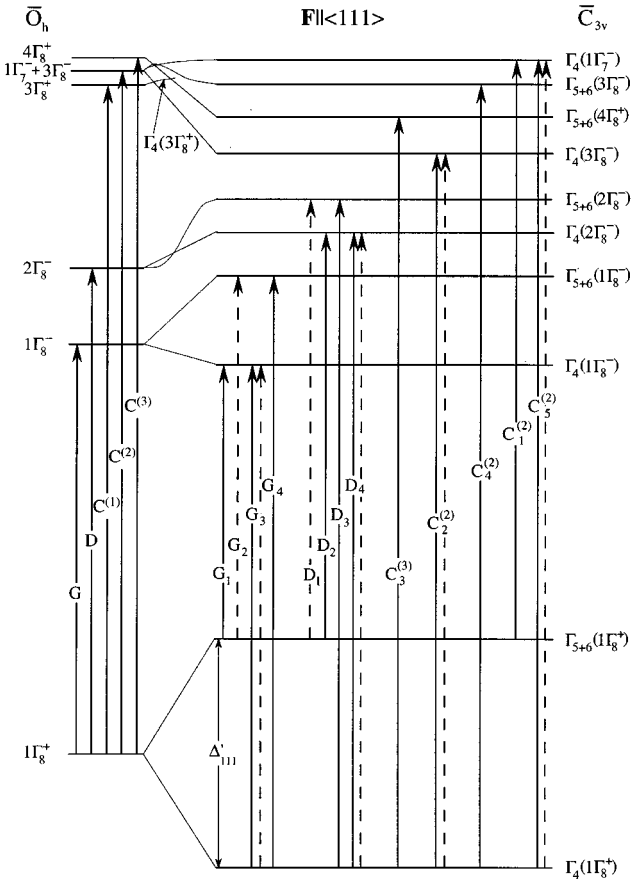

FIG. 5. Transitions for Ge(Zn^-) with $\mathbf{F}\|\langle 111\rangle$ at a stress of 200 MPa. Dashed lines are for $\mathbf{E}\|\mathbf{F}$; full lines are for $\mathbf{E}\perp\mathbf{F}$. $C_{4'}^{(1)}$, i.e., $\Gamma_4(1\Gamma_8^+)\rightarrow\Gamma_4(3\Gamma_8^+)$, is not observed at this stress; neither are G_1 and G_2. $C_1^{(2)}$ and $C_5^{(2)}$ may not have the same excited state (see text). The use of the symmetry labels of Ref. 21 for the unperturbed states permits unambiguous identification of the stress-induced states, which are labeled according to $\overline{C}_{3v}$ notation (Ref. 8), the appropriate subgroup of $\overline{T}_d$, rather than that of $\overline{D}_{3d}$. It should be noted that transitions between states of even parity, although forbidden under $\overline{O}_h$ symmetry and its subgroups with centers of inversion, are not forbidden for $\overline{T}_d$ and its derivatives since the center of inversion is not part of such groups. The unperturbed site symmetry of a substitutional acceptor is $\overline{T}_d$.

fits, the components D_2 and D_4, whose stress dependences are almost linear, yield intercepts that are the same as the unperturbed value, within experimental error. Thus it would appear that the force produced by the weights is all transmitted to the sample and hence the zero-stress value is also included in the least-squares fits as shown in Fig. 4.

The *D* line at low stress yields two components for $\mathbf{E}_\|$, the extreme energy components D_1 and D_4. At low stress only two components are observed for $\mathbf{E}_\perp$, whereas three are allowed.[8] At higher stress the higher-energy component for $\mathbf{E}_\perp$ separates into two components as repulsion increases between sublevels of the final states of the *D* and *G* lines.[10] Thus at low stress the high-energy component for $\mathbf{E}_\perp$ consists of two unresolved transitions, D_3 and D_4. From Fig. 4, it is seen that at high stress the D_4 component is common to both polarizations and thus, from the selection rules, must be the transition $\Gamma_4\rightarrow\Gamma_4$. Hence the order of the substates of both the ground and excited state involved are obtained unambiguously. Application of the selection rules produces the observed disposition of *D* components. The corresponding energy-level diagram for a stress of 200 MPa is given in Fig. 5. In this figure, Δ'_{111} designates the splitting of the ground state.[8]

Previously,[10,11] it was demonstrated that the stress enhancement of G_4 is due to interaction between the Γ_{5+6} sublevels of the final substates of the *D* and *G* transitions (see Fig. 5); this is also the origin of the decrease in the intensity of D_3. (The origin of the growth of G_3 requires a more complex explanation).[11] The repulsion between these two Γ_{5+6} states produces the crossings of D_4 by D_3 and D_2 by D_1 and hence the separation of D_3 from D_4 for $\mathbf{E}_\perp$ at higher stress. Interaction between the two excited Γ_4 substates is expected but is predicted[11] to be significantly smaller than that between the two Γ_{5+6} states, as is borne out by the almost linear stress dependence of D_2 and D_4 at low stress. This is consistent with the upper sublevel of the excited state of the *G* line being of Γ_{5+6} symmetry.[10] This ordering for the final state of the *G* line is given in Fig. 5 and is the basis for the labeling of the observed *G* components. The transitions G_1 and G_2 from the upper ground state are not observed, presumably because depopulation of this state

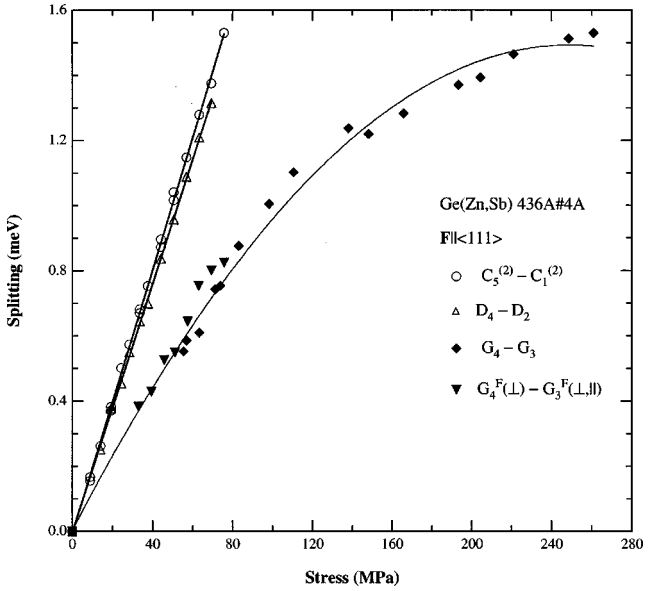

FIG. 6. Stress dependence of the energy spacing of D_2 and D_4 of Ge(Zn^-) for $\mathbf{F}\|\langle 111\rangle$; this spacing gives the ground-state splitting, Δ'_{111}. The energy difference of $C_1^{(2)}$ and $C_5^{(2)}$ is also given, as are the spacings of G_3 and G_4 and of $G_3^F(\perp,\parallel)$ and $G_4^F(\perp)$.

is well advanced before stress enhancement occurs. Thus G_3 corresponds to a transition to the Γ_4 excited substate and hence its energy should have an almost linear dependence on stress, as is the case. A G_3 component is allowed for $\mathbf{E}_\parallel$; in this work and BF76 there is very little evidence for this transition. For Ga in Ge, the intensity of $G_3(\mathbf{E}_\parallel)$ is almost zero for this orientation of $\mathbf{F}$.[28]

Only interactions between the two four-fold manifolds of the two Γ_8 excited states of the D and G lines have been considered. Numerical calculations for group III impurities[29] contain many more interactions and the results give a more complete picture of the behavior of the final states. Since the excited states of Ge(Zn^-) have energy spacings which are approximately four times larger than those of the group III impurities, stress-induced interactions of a given magnitude between corresponding excited states should occur at much larger stresses for Zn^-. In addition, the ground state for Zn^- lies about ten times further below its first excited state than is the case for the group III impurities and thus should be even less affected by mixing than the excited states.

The stress dependence of the C and D components should give the deformation potential constant of the ground state, $1\Gamma_8^+$, while the G and D components should give those of $1\Gamma_8^-$ and $2\Gamma_8^-$, respectively. Because of the complex nature of the C line, the determination of Δ'_{111} from the D line will be considered first. This splitting is the difference in energy of either D_3 and D_1 or D_4 and D_2. Since D_3 is not resolved at low stresses and D_1 is not observed at high stresses (due to thermal depopulation of the upper ground-state sublevel) only D_2 and D_4 can be used. The stress dependence of their splitting as determined from only the data obtained with lead weights is shown in Fig. 6. The straight line drawn through the data is the result of a least-squares fit, including the point at (0,0), and yields the value of Δ'_{111} for the ground state $1\Gamma_8^+$, and hence the value of d' given in Table III for this state. The linearity of the relation between Δ'_{111} and S is another clear indication that, for the stresses involved, interactions from other states produce very little effect on the splitting of the ground state.

The determination of Δ_{111}^G and Δ_{111}^D, the splittings of the $1\Gamma_8^-$ and $2\Gamma_8^-$ states, respectively, is not as simple as for Δ'_{111}, since now at least one of the stress-induced substates has a nonlinear dependence on S. The stress dependence of the energy difference of G_3 and G_4 is also given in Fig. 6; the curve is a quadratic least-squares fit to the data. The behavior is very similar to that obtained for Ga in Ge,[28] but the effects in Ge(Zn^-) occur at much higher stress, as expected. The value of Δ_{111}^G is the linear term in the fit to the G data in Fig. 6 and gives the value of d'_G shown in Table III for the $1\Gamma_8^-$ excited state; this deformation potential constant has not been determined before.

The value of Δ_{111}^D is much more inaccurate than that for Δ_{111}^G. Again, only one pair of components can be used, D_1

TABLE III. Experimental deformation potential constants for Zn^- in Ge, Ga in Ge, and theoretical deformation potential constants for group III impurities in germanium. Units are eV.

	Ge(Zn^-)				Ge(Ga)		Ge(III)	
	This work		Previous work[a]		Previous work		Theory[b]	
State	b'	d'	$\lvert b'\rvert$	d'	b'	d'	b'	d'
$1\Gamma_8^+$	-0.727 ± 0.008[c]	-2.267 ± 0.012	0.75 ± 0.02	-2.32 ± 0.09	-1.20 ± 0.01[d]	-2.91 ± 0.06[e]	-1.20	-2.68
$1\Gamma_8^-$		-1.43 ± 0.05			0.213 ± 0.007[e]	-1.10 ± 0.04[e]	0.22	-1.14
$2\Gamma_8^-$	0.599 ± 0.004	0.33 ± 0.05	0.65 ± 0.02		0.53 ± 0.03[d]	$<\lvert 0.06\rvert$[e]	0.50	0.18
$3\Gamma_8^-$	~ 0.73[f]	-1.67 ± 0.08			0.53 ± 0.02[d]		0.59[d]	-1.10
$3\Gamma_8^+$	$-$	$+$			-0.22 ± 0.05[d]		0.01	-0.40
$4\Gamma_8^+$	$+$	$+$						

[a]Reference 10.
[b]Reference 29.
[c]Obtained from the D-line data; using line $C^{(2)}$ data give -0.718 ± 0.008 (see text).
[d]Reference 30.
[e]Reference 28.
[f]Estimated from line $C^{(2)}$ (see text).

and D_2. Their energy separation is very small and increases at first and then decreases (see Fig. 4). A quadratic fit over the range 0–70 MPa yields Δ_{111}^{D}, the linear term, and hence d_D' for the excited state $2\Gamma_8^-$, a quantity not determined previously.

For stresses up to ~25 MPa, the C line gives rise to two well-defined components for $\mathbf{E}_\perp$ and one for $\mathbf{E}_\parallel$ (see Fig. 4). Beyond this stress the higher-energy unpolarized component, $C_5^{(2)}$ develops the well-resolved low-energy feature $C_{4'}^{(1)}$. This appears only as a shoulder for $\mathbf{E}_\perp$ and disappears at stresses above ~100 MPa. The three lowest-energy data points for $C_{4'}^{(1)}$ shown in Fig. 4 have been obtained by fitting Lorentzians to the absorption lines and are believed to be less reliable than the others. It will be argued below that this component is not $C_4^{(2)}$, which appears at higher stress only for $\mathbf{E}_\perp$, but, again, on the low-energy side of $C_5^{(2)}$ (see Fig. 4). At stresses above ~70 MPa, two additional components, $C_2^{(2)}$ and $C_3^{(3)}$, are observed for $\mathbf{E}_\perp$; $C_2^{(2)}$ is also observed for $\mathbf{E}_\parallel$. Similar details to the above are exhibited in Figs. 4–6 of BF76.

The relative intensities, polarization, and depopulation characteristics of the C components at low stress ($S \lesssim 25$ MPa) are typical of the behavior of either a $\Gamma_8(\overline{T}_d) \rightarrow \Gamma_6(\overline{T}_d)$ or a $\Gamma_8(\overline{T}_d) \rightarrow \Gamma_7(\overline{T}_d)$ transition for $\mathbf{F} \| \langle 111 \rangle$. Under such a perturbation, both $\Gamma_6(\overline{T}_d)$ and $\Gamma_7(\overline{T}_d)$ reduce to $\Gamma_4(\overline{C}_{3v})$ and the transitions $\Gamma_{5+6} \rightarrow \Gamma_4(\mathbf{E}_\perp)$, $\Gamma_4 \rightarrow \Gamma_4(\mathbf{E}_\perp)$, and $\Gamma_4 \rightarrow \Gamma_4(\mathbf{E}_\parallel)$ have relative intensities 3:1:4, respectively.[8] This strongly supports the argument that the main C line, $C^{(2)}$, has a Γ_7^- state as part of its final state (see Fig. 4 of BF76). Consequently, the low-stress C components are labeled $C_1^{(2)}$ and $C_5^{(2)}$ (see Fig. 5). That these two components stem from $C^{(2)}$ is given further support from the results of linear fits to their energies in the stress range 0–80 MPa, for which only the weights were used. These give intercepts for $C_1^{(2)}$ and $C_5^{(2)}$ that are very close to the energy of the $C^{(2)}$ line at zero stress. Linear fits to $C_2^{(2)}$ and $C_3^{(3)}$ up to ~200 MPa (including the data of Fig. 9 of BF76 for $C_3^{(3)}$) unambiguously identify these two components as stemming from $C^{(2)}$ and $C^{(3)}$, respectively.

It remains to justify the identification of the parent lines of $C_{4'}^{(1)}$ and $C_4^{(2)}$. Since $C_1^{(2)}$, $C_2^{(2)}$, and $C_5^{(2)}$ all appear to originate from $C^{(2)}$, the final state cannot be simply $1\Gamma_7^-$. As the theory places no other Γ_6 or Γ_7 state near $1\Gamma_7^-$, it is assumed that a Γ_8 state is in coincidence with $1\Gamma_7^-$, giving $\Gamma_4(1\Gamma_7^-)$, $\Gamma_4(\Gamma_8)$, and $\Gamma_{5+6}(\Gamma_8)$ as the stress-induced final substates of $C^{(2)}$, where it is necessary to identify which Γ_8 state this is. Both $C_2^{(2)}$ and $C_5^{(2)}$ are observed in each polarization thus exhausting all allowed transitions of the type $\Gamma_4 \rightarrow \Gamma_4$. However, $C_{4'}^{(1)}$ is also observed for both polarizations and hence must be a $\Gamma_4 \rightarrow \Gamma_4$ transition and, because of its energy, must originate from the lower ground state. If the three lowest data points for $C_{4'}^{(1)}$ are ignored as being relatively unreliable then a linear extrapolation of the stress dependence of $C_{4'}^{(1)}$ to zero stress gives an intercept that falls approximately midway between $C^{(1)}$ and $C^{(2)}$. It is thus assumed that $C_{4'}^{(1)}$ is derived from $C^{(1)}$ since another $\Gamma_4 \rightarrow \Gamma_4$ transition is now permitted whatever the nature of the final state of $C^{(1)}$. The fit to the stress dependence of the energy of $C_{4'}^{(1)}$, shown in Fig. 4, is a quadratic least-squares fit, omitting the three lowest-energy points but including the energy of $C^{(1)}$.

The component $C_4^{(2)}$ clearly originates from the lower ground substate, Γ_4, and, since it is only observed for $\mathbf{E}_\perp$, must be a $\Gamma_4 \rightarrow \Gamma_{5+6}$ transition, where the Γ_{5+6} excited state originates from the Γ_8 state which is assumed to be coincident with $1\Gamma_7^-$. (It is not clear if the nature of its polarization can be used to argue that it is not $C_{4'}^{(1)}$, which occurs for both polarizations, since the clearly seen stress enhancement of $C_4^{(2)}$ may affect the intensities differently for the two polarizations.)

Before completing the discussion of $C_4^{(2)}$, it is necessary to return to $C_1^{(2)}$ and $C_5^{(2)}$, whose energy spacing should be Δ_{111}'. The spacing of $C_1^{(2)}$ and $C_5^{(2)}$ as a function of stress is shown in Fig. 6 where it is seen to be larger than that of D_2 and D_4. It might be that either $C_1^{(2)}$ or $C_5^{(2)}$ (or both) are composed of unresolved components and, since no such ambiguity exists for the D components, the value of Δ_{111}' obtained from the latter can be taken as correct. It might be conjectured that, since the energy spacing of $C_1^{(2)}$ and $C_5^{(2)}$ is greater than Δ_{111}', the $\Gamma_{5+6}(\Gamma_8)$ stress-induced excited substate of $C_4^{(2)}$ discussed above has an energy initially slightly higher than that of $\Gamma_4(1\Gamma_7^-)$. Thus, at lower stress $C_5^{(2)}(\mathbf{E}_\perp)$ could be a mixture of two transitions. However, the energies of $C_5^{(2)}(\mathbf{E}_\perp)$ and $C_5^{(2)}(\mathbf{E}_\parallel)$ are found to be the same and no such mixture appears to be possible for the latter. Also, it is difficult to see how $C_1^{(2)}(\mathbf{E}_\perp)$ can be a compound transition as the transition $\Gamma_{5+6}(1\Gamma_8^+) \rightarrow \Gamma_{5+6}(\Gamma_8)$ is not allowed for $\mathbf{E}_\perp$.[8] Thus, the reason that the $C^{(2)}$ and D components fail to give the same value of Δ_{111}' is not understood but the value obtained directly from the D components will be taken as correct.

The stress dependence of the energies of the states involved in the G, D, and C lines is given in Fig. 7. The equations obtained from fits to the experimental energies have been used to generate this figure, assuming that the energies of the two ground-state substates have a linear behavior and assigning any hydrostatic terms to the excited states. The behavior depicted in Fig. 5 as the states change from their zero-stress energies to those at 200 MPa has been obtained from Fig. 7. It is seen that the repulsion producing the complex stress dependence of D_3 and $C_4^{(2)}$ at the larger stresses (see Fig. 4) appears to be caused by an interaction between $\Gamma_{5+6}(2\Gamma_8^-)$ and the Γ_{5+6} final state of $C_4^{(2)}$. This is presumably the reason why the intensity of D_3 decreases much more rapidly with stress than predicted.[11] This is a large effect, suggesting that the Γ_8 state almost coincident with $1\Gamma_7^-$ is $3\Gamma_8^-$ (as depicted in Fig. 7) and not $3\Gamma_8^+$, since interactions between states of opposite parity are expected to be small. This disagrees with the previous assignment[12] of $3\Gamma_8^-$ as the final state of $C^{(1)}$. This coincidence is the same as for the C line of Ga in Ge.[30] In constructing Fig. 7, interactions between odd- and even-parity states have been taken to be zero; thus states of opposite parity are shown as crossing even if the spatial part has the same symmetry. Such interactions, if they do exist, may be difficult to observe

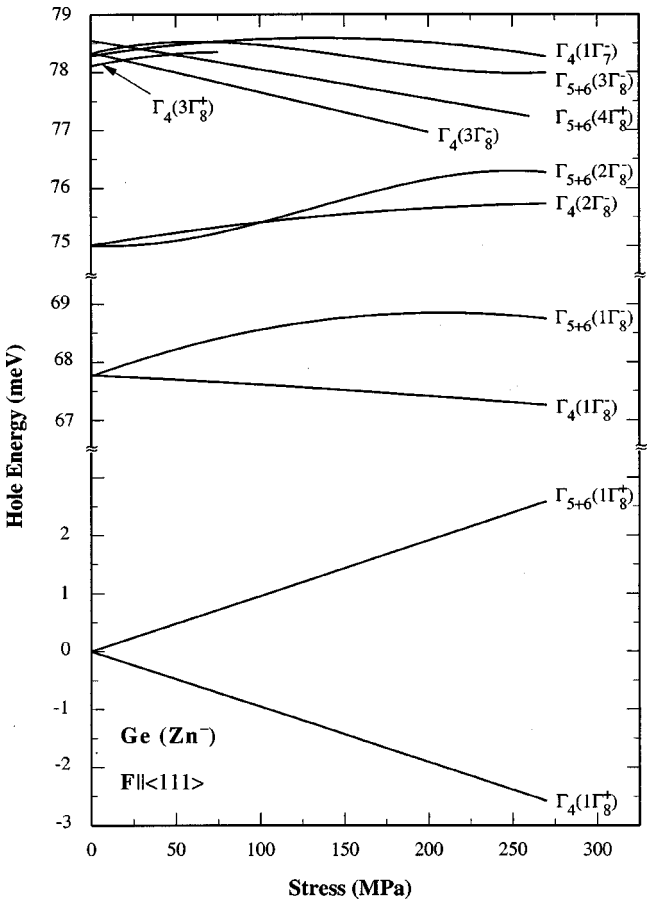

FIG. 7. Behavior of the ground state and the final states of the *G*, *D*, and *C* lines of Ge(Zn^-) for $\mathbf{F}\|\langle 111\rangle$. See text for details.

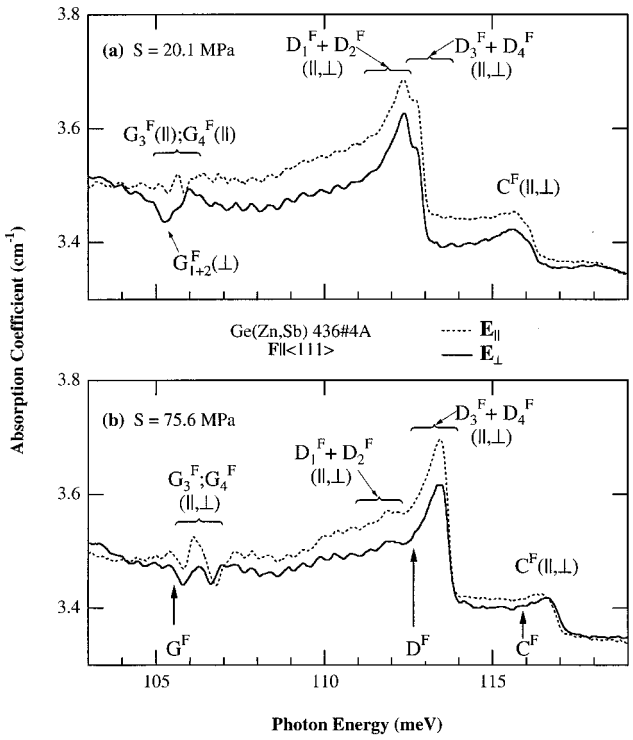

FIG. 8. Fano spectrum of Ge(Zn^-) for $\mathbf{F}\|\langle 111\rangle$. (a) Stress of 20.1 MPa. (b) Stress of 75.6 MPa. The vertical arrows in (b) give the positions of $h\nu_0$ for G^F, D^F, and C^F.

experimentally. The transitions assigned to the *C* components are included in Fig. 5 except for $C_{4'}^{(1)}$, which is the transition $\Gamma_4(1\Gamma_8^+)\rightarrow\Gamma_4(3\Gamma_8^+)$ for both polarizations.

The energies of the $C_1^{(2)}$ transitions have not been used in the construction of Fig. 7 since it is not clear that $C_1^{(2)}$ and $C_5^{(2)}$ have a common excited state; $C_5^{(2)}$ was used to give the stress dependence of $\Gamma_4(1\Gamma_7^-)$. At low stress, $\Gamma_{5+6}(3\Gamma_8^-)$ has an energy that is slightly higher than that of $\Gamma_4(1\Gamma_7^-)$. This follows from the cubic fit made using $C^{(2)}$ and the three data points for its component $C_4^{(2)}$ (see Fig. 4). This provides a state with the correct energy close to $\Gamma_4(1\Gamma_7^-)$, which might broaden the $C_1^{(2)}$ and $C_5^{(2)}$ components; however, it has been argued above that this cannot be the case. If a fit is made to the more extensive data of Fig. 9 of BF76 for $C_4^{(2)}$ a similar result is obtained except that $\Gamma_{5+6}(3\Gamma_8^-)$ lies further above $\Gamma_4(1\Gamma_7^-)$ at low stress than is shown in Fig. 7.

Deformation potential constants determined for the states $1\Gamma_8^+$, $1\Gamma_8^-$, $2\Gamma_8^-$, and $3\Gamma_8^-$ from the values obtained for Δ_{111}', Δ_{111}^G, Δ_{111}^D, and $\Delta_{111}^C(3\Gamma_8^-)$, respectively, are given in Table III. For comparison, the values obtained previously[10] and the experimental[28,30] and calculated[29] values for the corresponding group III states are also included. The signs of the constants are deduced from the ordering of the substates involved in each case.[8] From the considerations above regarding the *C* lines, the signs of $3\Gamma_8^+$ and $4\Gamma_8^+$ can be found; these are also included in Table III. The signs of the deformation potential constants for Zn^-, where measured, are the same as those for Ga, while the sign of $d'(3\Gamma_8^+)$ is opposite to that calculated for the corresponding state of a group III impurity.[29]

Even though the final state of the moderately intense *B* line is almost certainly $4\Gamma_8^-$, the stress pattern of this transition is remarkably featureless. This prevents a conclusive identification of the excited state.

b. Fano resonances. The effect of $\mathbf{F}\|\langle 111\rangle$ on the Fano resonances is shown in Figs. 3 and 8; preliminary results and the pertinent selection rules have been presented elsewhere.[12,27] The correlation between the Fano components and the parent $p_{3/2}$ components is illustrated in Fig. 3; the data for the two series were obtained at slightly different stresses. At 80 MPa the splitting of the phonon for $\mathbf{F}\|\langle 111\rangle$ is ~0.023 meV,[31] while the shift in its energy is also very small. Qualitatively the behavior of the Fano resonances correlates well with that of the $p_{3/2}$ transitions.

Before commenting on the detailed behavior of the components of the resonances, it is necessary to establish their quantitative evolution. Because of the broadness of these features, this is somewhat difficult when several components overlap, as is usually the case. A method has been described previously[14] by which the parameters of an isolated resonance may be determined; this will be called the ''straight-line'' (*l*) method. This is successful in analyzing unperturbed features but is of limited use in analyzing stress-split resonances. The dominant feature of a highly asymmetric resonance is its maximum, or peak (*p*). The dependence of *p* on stress can be more readily determined than that of $h\nu_0$ (the value of $h\nu$ at $\varepsilon=0$),[13] except for isolated components, such as the high-energy component of D^F. For D_{3+4}^F, it is possible to follow the stress dependence of both $h\nu_0$ and *p*; the

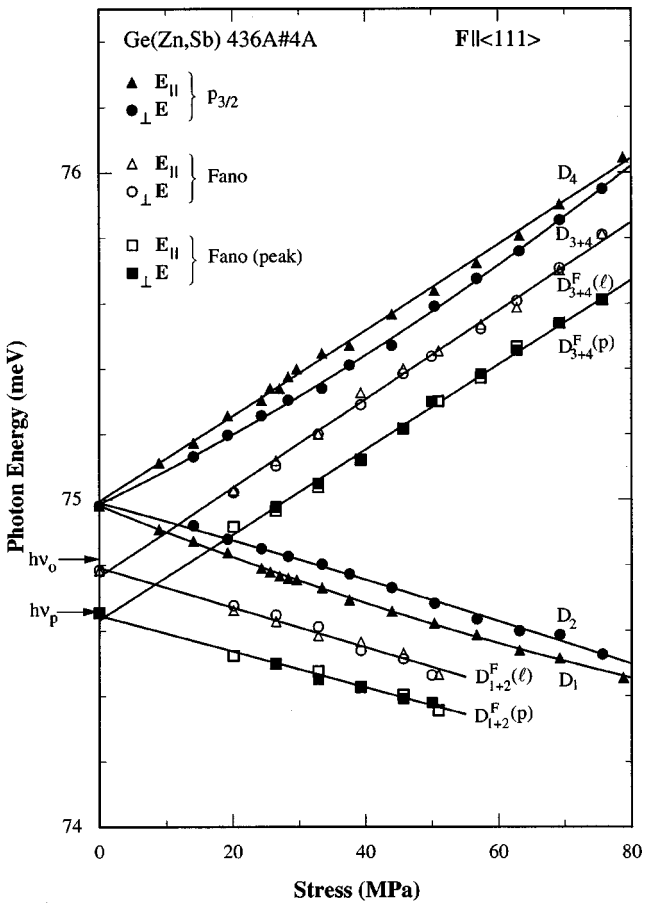

FIG. 9. Stress dependence of D and D^F components of Ge(Zn^-) for $\mathbf{F}\|\langle 111\rangle$. The energies of the latter have been reduced by 37.83 meV for ease of comparison. See text for the meanings of l and p.

results are given in Fig. 9. No data are included for D^F_{1+2} beyond ~50 MPa since depopulation of the upper stress-induced bound-hole ground state reduces its intensity to that of the weak interference fringes observed in all measurements. The unperturbed energy of $D^F(p)$ is 112.455 ± 0.005 meV, while the data labeled $D^F_{3+4}(l)$ are those from the l method and give $h\nu_0$. Also included in Fig. 9 are similar results for D^F_{1+2} although these are not expected to be as precise as those for D^F_{3+4}. It is seen that a given peak has a stress dependence that is close to that of the corresponding $h\nu_0$. This is to be expected if the value of q is independent of stress since the peak occurs at $\varepsilon = 1/q$. The straight lines drawn through the data for the components of D^F in Fig. 9 are the results of least-squares fits and are

$$h\nu_{1+2}(p) = (112.476 \pm 0.005) - (0.0055 \pm 0.0001)S \text{ meV},$$

$$h\nu_{0,1+2}(l) = (112.622 \pm 0.005) - (0.0061 \pm 0.0002)S \text{ meV},$$

$$h\nu_{3+4}(p) = (112.462 \pm 0.006) + (0.0130 \pm 0.0001)S \text{ meV},$$

$$h\nu_{0,3+4}(l) = (112.595 \pm 0.005) + (0.0135 \pm 0.0001)S \text{ meV},$$

where S is in MPa. Thus, the stress dependence of the energy of these asymmetric components is reasonably well represented by the behavior of their peaks.

In the above two examples, the stress dependence of the energies of the Fano components has been assumed to be linear; however, the behavior of the parent D components, particularly D_1 and D_3, is not linear. Each observed Fano feature is a mixture of several components involving the phonons and the parent line. The manner in which the latter behaves is shown in Fig. 4; for comparison, this behavior is included in Fig. 9. If the energies of D_{3+4} and D_4 are averaged and a linear fit made, the slope is 0.0129 meV/MPa, which is in good agreement with the corresponding Fano data. Similarly, the slope of the line fitted to the average of D_1 and D_2 is -0.0064 meV/MPa, which is close to the Fano results obtained from both the l and p methods.

The behavior of G^F for $\mathbf{F}\|\langle 111\rangle$ is significantly different from that of D^F. At low stress, for $\mathbf{E}_\perp$, the resonance shifts to lower energies and is labeled $G^F_{1+2}(\perp)$. At $S \gtrsim 30$ MPa, this component is no longer observed. For $S \gtrsim 40$ MPa, two antiresonances appear at energies higher than G^F at zero stress (see Figs. 3 and 8) and are labeled $G^F_3(\perp)$ and $G^F_4(\perp)$ (see below). It was not possible to determine precisely the stress at which these two antiresonances appear due to the presence of the interference fringes. There appears to be evidence of the two antiresonances at ~39 MPa while at ~46 MPa there is no doubt of their presence (see Fig. 3). For $\mathbf{E}_\|$, two resonances appear at the lowest stress used, one lower in energy than the zero-stress resonance and the other higher; the latter is labeled $G^F_4(\|)$. As stress increases, the lower-energy resonance disappears (see Fig. 8) while another one, $G^F_3(\|)$, appears at a higher energy than the unperturbed resonance (see Figs. 3 and 8). The latter component also seems to appear at ~39 MPa and to be an antiresonance, similar to the $\mathbf{E}_\perp$ components. The higher-energy component, $G^F_4(\|)$, observed for $\mathbf{E}_\|$ at all stresses does not appear to be an antiresonance and has a shape suggesting $q<0$ and so of opposite sign to the q of the unperturbed resonance.

In order to obtain quantitative information about the components of G^F, it is necessary to consider their shapes. If $|q|>1$, the peak of the resonance is the sharper feature; if $|q|=1$, the maximum and minimum are equally sharp; if $|q|<1$ the minimum will be the sharper; if $q=0$ (a pure antiresonance) the only feature is the minimum that coincides with $\varepsilon = 0$ and thus $h\nu_{\min} = h\nu_0$. All G^F components appear to fall into the last two categories. Thus energies of their *minima* will be used to demonstrate their stress dependence. The results are given in Fig. 10 along with the behavior of the observed components of the parent G line. There are two zero-stress data points shown for G^F. The one of greater energy is $h\nu_0$ (see Table II), while the other is $h\nu_{\min}$, which is 0.18 meV lower in energy than $h\nu_0$.

First, from Fig. 10, it is noted that the data points for G^F_3 for both $\mathbf{E}_\|$ and $\mathbf{E}_\perp$ coincide at all stresses. This implies that q for this component is the same in both polarizations and, in particular, if one is a pure antiresonance so is the other. If a linear fit is made to the data for G^F_3 for both polarizations without including the zero-stress value of $h\nu_{\min}$, the intercept is close to the unperturbed value of $h\nu_{\min}$. If the latter value is included the fit is even better. The dependence of G^F_3 on S is ~3/4 that of G_3; it is tentatively concluded that G_3 is the parent of G^F_3. Secondly, it is found that the data for $G^F_4(\mathbf{E}_\perp)$ follow much more closely those of G_4 than do those

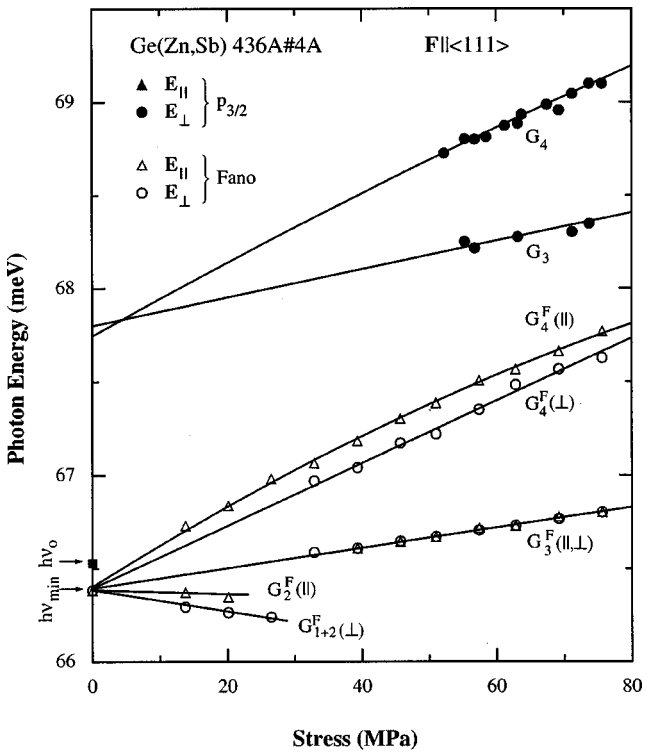

FIG. 10. Stress dependence of $p_{3/2}$ and Fano G components of Ge(Zn$^-$) for $\mathbf{F}\|\langle 111\rangle$. The energies of the minima of the G^F components are shown; these have been reduced by 39 meV for ease of comparison. The datum labeled $h\nu_{\min}$ is the energy of the minimum of G^F at $S=0$; $h\nu_0$ is defined in the text.

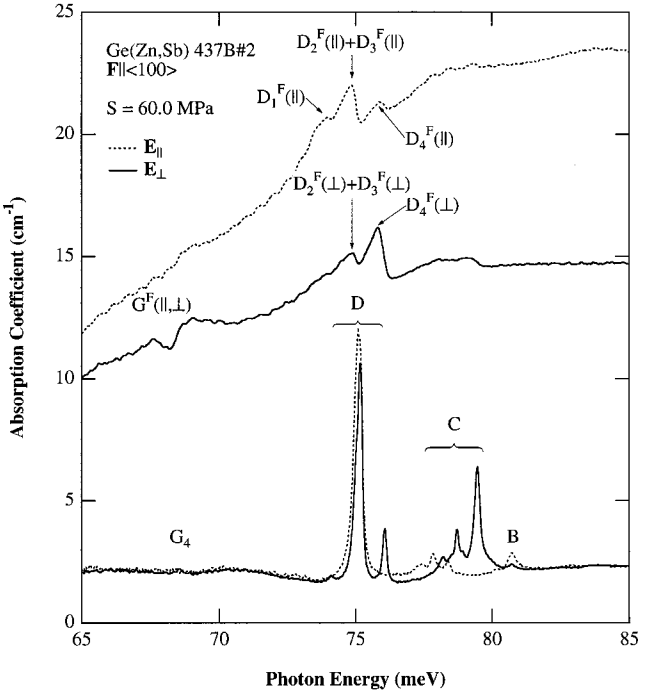

FIG. 11. The $p_{3/2}$ and Fano spectra of Ge(Zn$^-$) for $\mathbf{F}\|\langle 100\rangle$ and stress of 60.0 MPa.

of $G_4^F(\mathbf{E}_\|)$; the latter has a much larger quadratic term than either of the other two. The energy difference of $G_3^F(\mathbf{E}_\|,\mathbf{E}_\perp)$ and $G_4^F(\mathbf{E}_\perp)$ is plotted in Fig. 6, from which it is seen that there is a close correspondence with the data for the difference in energy of G_3 and G_4. Within experimental error, the linear part of the fit to the former difference is the same as that obtained for the latter. Thirdly, the energy spacing at low stress between $G_2^F(\mathbf{E}_\|)$ and $G_4^F(\mathbf{E}_\perp)$ is very close in value to Δ'_{111}, implying that $G_2^F(\mathbf{E}_\|)$ has G_2 as its parent. The origin of the broad low-energy component for $\mathbf{E}_\perp$ is not clear but, since it lies between G_2^F and the energy at which G_1^F is predicted to occur, it could be the two unresolved components $G_1^F(\mathbf{E}_\perp)$ and $G_2^F(\mathbf{E}_\perp)$; this is the basis of the label in Fig. 10. These low-energy components are not observed as the stress increases because of depopulation effects.

Finally, it would appear that $G_4^F(\mathbf{E}_\|)$ has G_4 as its parent transition. If the above considerations for $G_4^F(\mathbf{E}_\perp)$ are correct and it is a pure antiresonance then its $h\nu_{\min}$ must coincide with its $h\nu_0$. Since the energy of the minimum of $G_4^F(\mathbf{E}_\|)$ is larger than that of $G_4^F(\mathbf{E}_\perp)$ then $q<0$ for the former, and the value of $h\nu_{\min}=h\nu_0$ for $G_4^F(\mathbf{E}_\perp)$ will determine the value of $h\nu_0$ for $G_4^F(\mathbf{E}_\|)$. Since the energy of the minimum of $G_4^F(\mathbf{E}_\|)$ varies nonlinearly with S, q for this component must vary with stress. It remains to determine why $G_4^F(\mathbf{E}_\|)$ behaves differently from the other observed G^F components; it might be noted that the parent component, $G_4(\mathbf{E}_\|)$, is forbidden in the $p_{3/2}$ series. It is conjectured that the mixing between the bound stress-induced substates, which produces the stress enhancement of the parent G components, leads to the variation observed. However, the consequence of this on D_3 is just as dramatic and yet D_{3+4}^F does not appear to be affected, although the data are more difficult to analyze because of the superposition of the two D components. There is not a very large mixing effect for the final state of G_3 and thus the value of q for G_3^F would not be expected to vary very much from this cause. On the other hand, if $q=0$ for G_3^F at all stresses, mixing would produce no effect.

2. Applied force along a ⟨100⟩ axis

a. $p_{3/2}$ spectrum. The behavior of the $p_{3/2}$ transitions for a compressive force along $\langle 100\rangle$ is illustrated in Fig. 11. The results are almost identical to those of BF76 except that for stresses $\geqslant$40 MPa, the D_2 and D_3 components for $\mathbf{E}_\perp$ are distinguished more clearly. The intensity of the D_2 component decreases with increasing stress as a result of depopulation of the upper stress-induced ground state, and as a consequence can be detected over only a limited range of stress. Since the D components were not well resolved, a Lorentzian curve-fitting program was used to obtain their energies. The C components are labeled according to the scheme described for $\mathbf{F}\|\langle 111\rangle$. See Fig. 12 which shows the stress dependence of all but the G transitions. The stress-induced G components, G_3 and G_4, start to appear at a stress of $\sim$45 MPa and their intensities increase with stress, but not as dramatically as for $\mathbf{F}\|\langle 111\rangle$. The calculations by Buczko[29] for group III impurities yield the same sign of b' for the final states of the D and G lines and thus predict that stress-induced states of the same symmetry are not adjacent to each other, unlike the case for $\mathbf{F}\|\langle 111\rangle$; this is presumably the reason for the observed smaller stress enhancement of the G components for $\mathbf{F}\|\langle 100\rangle$.

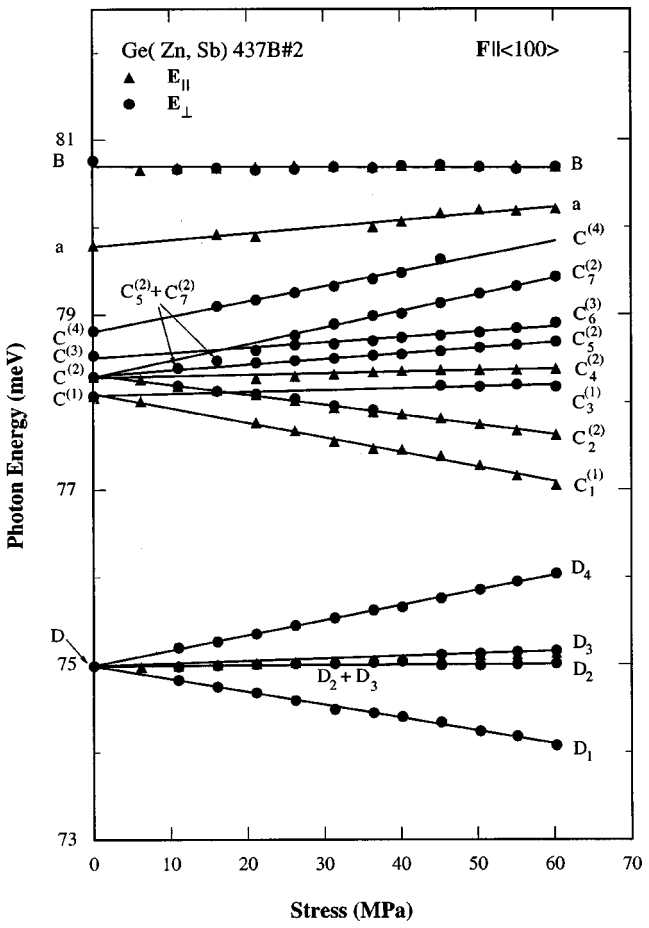

FIG. 12. Stress dependence of *D, C, a,* and *B* components of $Ge(Zn^-)$ for $\mathbf{F}\|\langle 100\rangle$.

The results given in Fig. 12 are much more detailed than those of BF76 over the same range of stress and permit a much better opportunity to follow the evolution of the *C* components. For this to be carried out as effectively as possible, the ground-state splitting must be obtained independently of the *C* lines. The splitting of the *D* line provides the only means for doing this. There is no ambiguity about the origin of the *D* components. The transition $1\Gamma_8^+ \rightarrow 2\Gamma_8^-$ splits into four components, two of which are allowed in both polarizations while the other two are only permitted for $\mathbf{E}_\perp$. It has been observed previously[9,10] that Δ'_{100} and Δ^D_{100} are not very different in value. This is the reason the two components D_2 and D_3, common to both polarizations, are difficult to resolve. From the selection rules and the experimental result that this pair of components are of intermediate energy it is deduced that b' and b'_D have opposite signs. It is not possible from the experimental behavior of the *D* line alone to determine the signs of the deformation constants, i.e., which of the two stress-induced substates is of lower energy—the one of $\Gamma_6(\overline{D}_{2d})$ symmetry or the one of $\Gamma_7(\overline{D}_{2d})$ symmetry.

Linear fits to the data for D_1 and D_4, without the inclusion of the zero-stress energy, yield intercepts that agree with the latter within experimental error. From these results it is clear that, for any of the data shown in Fig. 12, when a linear fit is made to a component whose parent line is unambiguous, the zero-stress energy of the parent can be included, and that when the energy difference between two such components is being considered the point (0, 0) can be included in the fit. A linear fit to the energy difference of D_1 and D_4 gives the value of $|\Delta'_{100}+\Delta^D_{100}|$; the result obtained is ~6% smaller than that given in BF76. Linear fits to the few data points for the spacings of D_1 and D_3, and D_3 and D_4, yield Δ'_{100} and Δ^D_{100}, respectively. The sum of these two agrees well with that obtained above directly from D_1 and D_4. These values of Δ'_{100} and Δ^D_{100} are ~4% and ~8% smaller, respectively, than those of BF76.

The spectrum of the *C* lines for $\mathbf{F}\|\langle 100\rangle$ is richer than that for $\mathbf{F}\|\langle 111\rangle$ and resembles that for Ga in Ge.[30] A linear fit to the data of Fig. 12 for $C^{(4)}$ without including the zero-stress value gives an intercept identical, within experimental error, to the zero-stress value. This clearly identifies the parent line of this component and thus the linear fit to $C^{(4)}$ shown in Fig. 12 includes the zero-stress value. In what follows, it is assumed that each *C* component has a linear dependence on stress. This assumption is well borne out in all cases, provided it is recognized that the two data points labeled $C_5^{(2)}+C_7^{(2)}$, occurring at ~11 and 16 MPa, are composed of two unresolved components (as implied by the label) and the energies of $C_5^{(2)}$ and $C_7^{(2)}$ at 21 MPa have been obtained by curve fitting. At the smaller stress, the energy of the compound component $C_5^{(2)}+C_7^{(2)}$ approaches that of $C_5^{(2)}$, indicating that it is the more intense component.

Linear fits to all components, omitting zero-stress values, give intercepts that clearly identify the parent lines in each case except for $C_3^{(1)}$. Considerations to be given later indicate that $C^{(1)}$ is the parent line of $C_3^{(1)}$. The zero-stress energy is now included in the linear fit to each component resulting in the straight-line fits shown in Fig. 12. If the energy spacings between each *C* component and those of higher energy are determined it is found that three pairs have values that are the same as or close to the value of Δ'_{100} determined from the *D* components. These pairs are $C_1^{(1)}$ and $C_3^{(1)}$, $C_2^{(2)}$ and $C_5^{(2)}$, and $C_4^{(2)}$ and $C_7^{(2)}$. The data points at 21 MPa have been omitted for the pair $(C_4^{(2)}, C_7^{(2)})$. Of the $C_2^{(2)}$ components, only those for $\mathbf{E}_\|$ were used since they are much more clearly defined than those for $\mathbf{E}_\perp$. The values obtained for Δ'_{100} from the *C* and *D* components are in excellent agreement. Deformation potential constants thus obtained are given in Table III.

These results indicate the transitions with common final states. The energies and stress dependence of the intensities of the extreme components are an indication of the ground-state sublevel involved. Together with the fits to the energies of the components and their polarizations, it is possible to construct an energy-level diagram that accounts for essentially all the observed transitions. This is given to scale in Fig. 13 for $S=50$ MPa with the ordering of the ground-state sublevels taken to be that predicted theoretically.[29] The value of b' for $3\Gamma_8^-$ and the signs of $b'(3\Gamma_8^+)$ and $b'(4\Gamma_8^+)$ have been determined on the basis of this construction and are included in Table III.

The construction of Fig. 13 will be discussed. First, since at least four distinct components are attributed to $C^{(2)}$ and their energies and polarizations are not compatible with either a single Γ_7 state or a single Γ_8 state as the parent excited

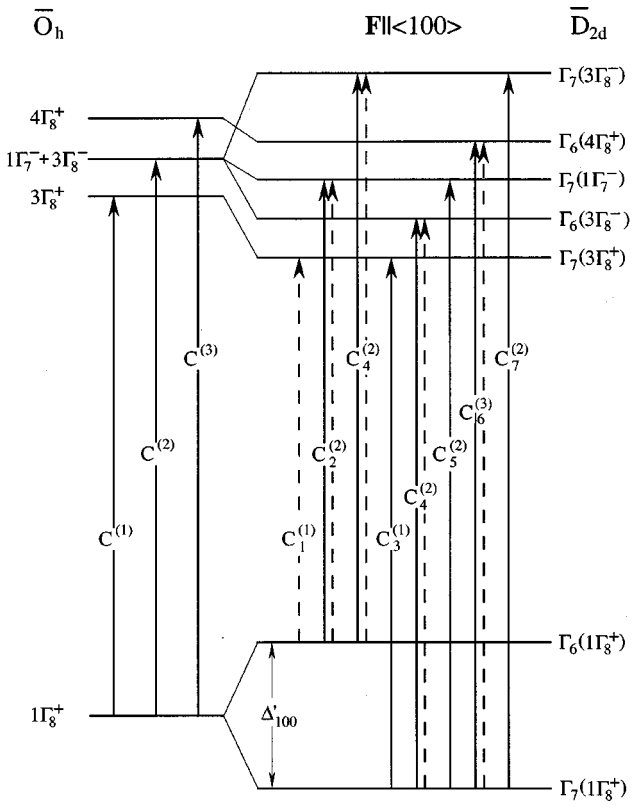

FIG. 13. Observed C transitions, their components, and origins for Ge(Zn^-) with $\mathbf{F}\|\langle 100\rangle$ at stress of 50 MPa. Dashed lines are for $\mathbf{E}\|\mathbf{F}$; full lines are for $\mathbf{E}\perp\mathbf{F}$. $C^{(4)}$ is not included (see text). The labeling of the stress-induced states is in the spirit of that described in the caption to Fig. 5.

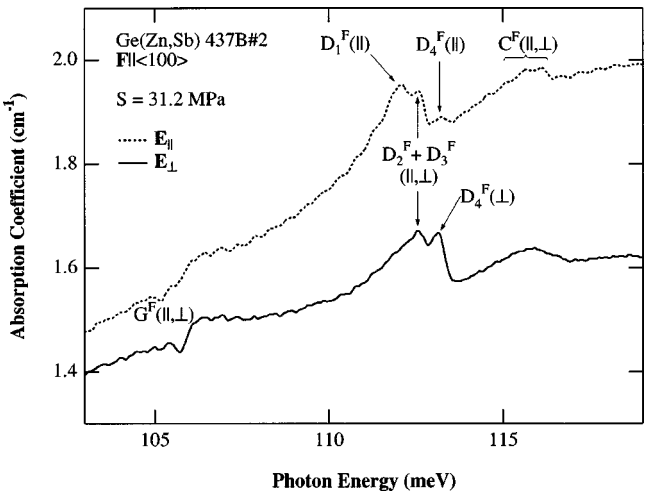

FIG. 14. The Fano spectrum of Ge(Zn^-) for $\mathbf{F}\|\langle 100\rangle$ at stress of 31.2 MPa.

state, it is concluded that the two states $1\Gamma_7^-$ and $3\Gamma_8^-$ together form this final state. The choice of $3\Gamma_8^-$ rather than $3\Gamma_8^+$ is based on the observation that most of the total intensity of the components is invested in those attributed to $C^{(2)}$ and it might be expected that the matrix elements would be significantly smaller for transitions to $3\Gamma_8^+$ than to $3\Gamma_8^-$, noting that very little mixing occurs for this direction of $\mathbf{F}$. Secondly, the component $C_4^{(2)}$ has been demonstrated to arise from the upper ground state and yet its intensity shows very little variation with stress. Thus it is concluded that this component is the superposition of two transitions, one from the upper ground state and another of almost the same energy from the lower ground state. If this is so, this is the only transition observed to $\Gamma_6(3\Gamma_8^-)$ and requires the $3\Gamma_8^-$ state to have the same deformation potential constant as the ground state. Thirdly, the previous results indicate that $C_6^{(3)}$ also appears for $\mathbf{E}_\|$ (see Fig. 13 of BF76) and thus its final state is labeled $\Gamma_6(4\Gamma_8^+)$. Fourthly, there are insufficient transitions seen to permit the energy of $\Gamma_6(3\Gamma_8^+)$ to be determined unless $C_3^{(1)}$ originates from the upper ground state, which is unlikely since this small but distinct component persists even at large stress (see BF76). Finally, the basis for distinguishing $\Gamma_7(1\Gamma_7^-)$ and $\Gamma_7(3\Gamma_8^-)$ needs to be explained. At low stress, the components $C_2^{(2)}(\mathbf{E}_\|)$ and $C_5^{(2)}(\mathbf{E}_\perp)$ appear to be the dominant ones while there is also a weak $C_2^{(2)}(\mathbf{E}_\perp)$ component. These have a pattern similar to that expected for a $\Gamma_8(\overline{T}_d)\rightarrow\Gamma_7(\overline{T}_d)$ transition.[8] In addition, it is predicted[24] that for group III impurities the intensity of the transition to $1\Gamma_7^-$ will be significantly stronger than that to $3\Gamma_8^-$ and, thus, at very low stress, the former should provide most of the intensity of the stress components. If this argument can be sustained, then the ordering of the ground-state sublevels is determined immediately. However, in this context, the growth of the intensity of $C_7^{(2)}$ needs to be understood.

The deductions regarding the nature of the components and excited states of $C^{(1)}$, $C^{(2)}$, and $C^{(3)}$ proposed in Fig. 13 have been made without reference to the interpretation given elsewhere[30] for the C line of Ga in Ge. However, there are clear correspondences between the stress-induced spectra of the two impurities. A comparison between the spectra shows that essentially all the components for $\mathbf{E}_\|$ ''freeze out'' at high stress leaving the dominant high-energy $\mathbf{E}_\perp$ components, while at low stress there is one main component for $\mathbf{E}_\|$. The accidentally superimposed transitions proposed here that comprise $C_4^{(2)}$ are well separated in the Ga spectra and their intensities exhibit a behavior which, when combined, would give that observed for $C_4^{(2)}$ of Zn^-. The transitions are separated for Ga because $b'(1\Gamma_8^+)$ is significantly larger than $b'(3\Gamma_8^-)$. In addition, the transition $\Gamma_7(1\Gamma_8^+)\rightarrow\Gamma_6(3\Gamma_8^+)$ appears only for $\mathbf{E}_\perp$ for Ga and is a very weak component while for Zn^- it is not observed at all; it is this transition that is required to establish the energy of the $\Gamma_6(3\Gamma_8^+)$ state.

b. Fano resonances. The piezospectra of the Fano resonances under a $\langle 100\rangle$ compression are presented in Fig. 11, which shows the correlation between the Fano series and the $p_{3/2}$ series. The behavior of the Fano spectra only at a lower stress is given in Fig. 14. The stress dependence of the energies of the peaks of the D^F components is given in Fig. 15 along with that of the D components. The lines are the results of linear least-squares fits. The datum point representing the zero-stress energy of the peak of D^F for this sample is at 112.49 ± 0.02 meV and has been included in the fits to D_1^F and D_{2+3}^F but not for D_4^F. The value for $h\nu_0$ (see Table II) is indicated in the figure.

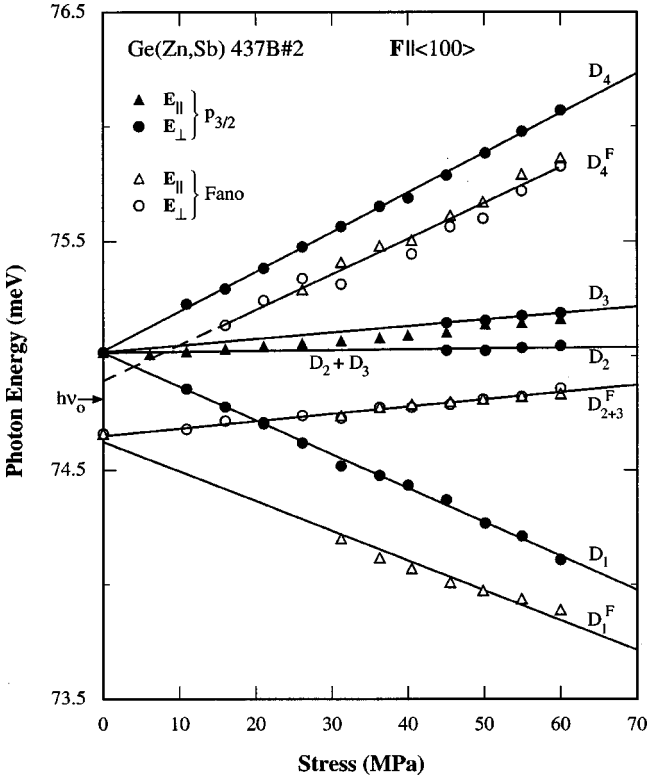

FIG. 15. Stress dependence of $p_{3/2}$ and Fano D components of Ge(Zn^-) for $\mathbf{F}\|\langle 100\rangle$. The energies of the peaks of the D^F components are shown, reduced by 37.83 meV for ease of comparison. The value of $h\nu_0$ for D^F is indicated.

If the spectra for the two polarizations are combined, they indicate qualitatively that the splitting of D^F follows that of the parent D line. While allowed by the selection rules,[27] it is interesting to observe how strong the D_1^F and D_4^F components are for $\mathbf{E}_\|$, since the parent bound-hole to bound-hole transitions are strictly forbidden. Also interesting is the decrease in intensity with increasing stress of D_{2+3}^F for $\mathbf{E}_\perp$. This is not the case for the supposedly same compound component for $\mathbf{E}_\|$. This might suggest that for $\mathbf{E}_\perp$ the component is mainly composed of D_2^F, whose intensity will diminish with increasing stress due to depopulation of the upper ground state, an effect clearly observed for $D_1^F(\mathbf{E}_\|)$. However, this conjecture is difficult to reconcile with the energy dependence of $D_{2+3}^F(\mathbf{E}_\perp)$ given in Fig. 15, where it is seen that the energy of the peak of this Fano component follows that of D_3 and not D_2.

From Fig. 15, it is seen that $D_1^F(\mathbf{E}_\|)$ has approximately the same stress dependence as D_1. The component $D_1^F(\mathbf{E}_\perp)$ is very weak, making it difficult to separate it from the small interference fringes which were present in all the results of this set. The stress dependence of D_4^F, which appears to be the same for both polarizations, is very interesting. The energy of the peak of this component follows the stress dependence of D_4 but extrapolates at zero stress to an intercept that is greater than $h\nu_0(D^F)$ (see Fig. 15); this is not understood.

The G^F components for $\mathbf{E}_\|$ are weak and difficult to separate from the interference fringes for stresses above $\sim$30 MPa. At lower stresses there is one component whose minimum is at lower energy than, and extrapolates to, the zero-stress minimum. There is one G^F component for $\mathbf{E}_\perp$; this is relatively strong but, again, because of the superimposed fringe pattern and the changing background absorption, it is difficult to determine its shape. The energy of the minimum of this component increases linearly with stress and, like D_4^F, extrapolates to a zero-stress value that is higher in energy than $h\nu_0$. Because of the lack of data for the behavior of the parent G components at the low stresses involved, it is not possible to identify with which of the latter the former is associated. Analysis of the C^F components is also difficult; these components are very broad, presumably because of the number of overlapping components arising from the parent C line.

As is the case for $\mathbf{F}\|\langle 111\rangle$, the energy of the zone-center optical phonons is known to split and shift but, again, these effects are small at the stresses used here. For example, for $\mathbf{F}\|\langle 100\rangle$ at 200 MPa a splitting of only 0.02 meV occurs.[31] The width of the Fano components makes such a small splitting unobservable at the stresses used.

IV. CONCLUSION

A state-of-the-art spectrometer has permitted more detailed and accurate $p_{3/2}$ absorption spectra of Ge(Zn^-) to be obtained than previously. The results on the piezospectroscopic behavior for the G and D transitions of the $p_{3/2}$ series are in excellent agreement with those reported previously. The origin of the complex, closely spaced C transitions has been partly clarified by examining their stress behavior. The first three lines of the C complex, $C^{(1)}$, $C^{(2)}$, and $C^{(3)}$, have the final states $3\Gamma_8^+$, $1\Gamma_7^- + 3\Gamma_8^-$, and $4\Gamma_8^+$, respectively, in reasonable agreement with theory. More reliable deformation potential constants of some energy states have been obtained by analyzing well-defined spectral components.

The Fano resonances of Ge(Zn^-) show typical Fano line shapes. These piezospectroscopic observations of Fano resonances of acceptors in Ge reveal that the resonant states exhibit behavior similar to that of their parent transitions in the $p_{3/2}$ series, although some interesting anomalies remain unexplained. The phonon splittings due to stress are too small to be determined from the behavior of the Fano stress components in the experiments reported here. The selection rules for $p_{3/2}$ transitions are greatly relaxed for the phonon-assisted Fano features, resulting in the observation of several striking phenomena; for example, the observed intensities of some of the stress-induced Fano components whose parent components are strictly forbidden. Another interesting effect is the way in which the resonance shape changes for the components of G^F, particularly for $\mathbf{F}\|\langle 111\rangle$.

ACKNOWLEDGMENTS

The work was supported in part by the Australian Research Council and the University of Wollongong Board of Research and Postgraduate Studies.

[1] P. Fisher and H. Y. Fan, Phys. Rev. Lett. **2**, 456 (1959).
[2] F. Bassani, G. Iadonisi, and B. Preziosi, Rep. Prog. Phys. **37**, 1099 (1974); M. Altarelli and F. Bassani, in *Handbook of Semiconductors*, edited by W. Paul (Amsterdam, North Holland, 1980), Vol. 1.
[3] S. T. Pantelides, Rev. Mod. Phys. **50**, 797 (1978).
[4] A. K. Ramdas and S. Rodriguez, Rep. Prog. Phys. **44**, 1297 (1981).
[5] R. Buczko and F. Bassani, in *Proceedings of the Third International Conference on Shallow Impurities in Semiconductors*, edited by B. Monemar, IOP Conf. Proc. No. 95 (Institute of Physics and Physical Society, London, 1989), p. 107; (private communication).
[6] R. Buczko and F. Bassani, Phys. Rev. B **45**, 5838 (1992).
[7] P. Fisher and H. Y. Fan, Phys. Rev. Lett. **5**, 195 (1960).
[8] S. Rodriguez, P. Fisher, and F. Barra, Phys. Rev. B **5**, 2219 (1972); **7**, 2889 (1972).
[9] F. Barra, P. Fisher, and S. Rodriguez, Phys. Rev. B **7**, 5285 (1973).
[10] N. R. Butler and P. Fisher, Phys. Rev. B **13**, 5465 (1976). Note that, where convenient, in the text this publication will be designated as BF76.
[11] K. J. Duff, P. Fisher, and N. R. Butler, Aust. J. Phys. **33**, 73 (1980).
[12] G. Piao, R. A. Lewis, and P. Fisher, Mater. Sci. Forum **65&66**, 313 (1991).
[13] U. Fano, Phys. Rev. **124**, 1866 (1961).
[14] G. Piao, R. A. Lewis, and P. Fisher, Solid State Commun. **75**, 835 (1990).
[15] See, for example, G. D. Watkins and W. B. Fowler, Phys. Rev. B **16**, 4524 (1977); M. Kleverman, J. Olajos, and H. G. Grimmeiss, *ibid.* **35**, 4093 (1987); **37**, 2613 (1988); M. Suezawa, A. Kasuya, K. Sumino, and Y. Nishina, J. Phys. Soc. Jpn. **57**, 4021 (1988).
[16] G. F. Koster, J. O. Dimmock, R. G. Wheeler, and H. Statz, *Properties of the Thirty-Two Point Groups* (MIT Press, Cambridge, MA, 1963).
[17] W. Kohn and D. Schechter, Phys. Rev. **99**, 1903 (1955).
[18] W. Kohn, in *Solid State Physics*, edited by F. Seitz and D. Turnbull (Academic, New York, 1957), Vol. 5, p. 257.
[19] D. Schechter, J. Phys. Chem. Solids **23**, 237 (1962).
[20] K. S. Mendelson and H. M. James, J. Phys. Chem. Solids **25**, 729 (1964).
[21] A. Baldereschi and N. O. Lipari, Phys. Rev. B **8**, 2697 (1973); **9**, 1525 (1974); in *Proceedings of the 13th International Conference on the Physics of Semiconductors*, edited by F. G. Fumi (Tipografia, Rome, 1976), p. 595; N. O. Lipari and A. Baldereschi, Solid State Commun. **25**, 665 (1978); N. O. Lipari, A. Baldereschi, and M. L. W. Thewalt, *ibid.* **33**, 277 (1980).
[22] V. J. Tekippe, H. R. Chandrasekhar, P. Fisher, and A. K. Ramdas, Phys. Rev. B **6**, 2348 (1972).
[23] C. A. Freeth (private communication).
[24] R. Buczko and F. Bassani, Phys. Rev. B **45**, 5838 (1992).
[25] Yu. A. Kurskii, Phys. Rev. B **48**, 5148 (1993).
[26] V. Fiorentini and A. Baldereschi, Solid State Commun. **69**, 953 (1989).
[27] G. Piao, R. A. Lewis, and P. Fisher, in *Proceedings of the 21st International Conference on the Physics of Semiconductors*, edited by Ping Jiang and Hou-Zhi Zheng (World Scientific, Singapore, 1992), p. 1609.
[28] A. D. Martin, P. Fisher, C. A. Freeth, E. H. Salib, and P. E. Simmonds, Phys. Lett. **99A**, 391 (1983).
[29] R. Buczko, Nuovo Cimento D **9**, 669 (1987).
[30] R. E. M. Vickers, P. Fisher, and C. A. Freeth, Solid State Commun. **65**, 271 (1988).
[31] F. Cerdeira, C. J. Buchenauer, F. H. Pollak, and M. Cardona, Phys. Rev. B **5**, 580 (1972).
[32] J. Menéndez and M. Cardona, Phys. Rev. B **29**, 2051 (1984).